Role of the DELSEED Loop in Torque Transmission of F_1-ATPase

Mizue Tanigawara,[†‡] Kazuhito V. Tabata,[‡**] Yuko Ito,[§] Jotaro Ito,[†‡] Rikiya Watanabe,[‡] Hiroshi Ueno,[¶] Mitsunori Ikeguchi,[§] and Hiroyuki Noji[†‡*]

[†]Graduate School of Frontier Bioscience, Osaka University, Osaka, Japan; [‡]Department of Applied Chemistry, Graduate School of Engineering, The University of Tokyo, Tokyo, Japan; [§]Graduate School of Nanobioscience, Yokohama City University, Yokohama, Japan; [¶]Department of Physics, Faculty of Science and Engineering, Chuo University, Tokyo, Japan; and **PRESTO, Japan Science and Technology Agency, Tokyo, Japan

ABSTRACT F_1-ATPase is an ATP-driven rotary motor that generates torque at the interface between the catalytic β-subunits and the rotor γ-subunit. The β-subunit inwardly rotates the C-terminal domain upon nucleotide binding/dissociation; hence, the region of the C-terminal domain that is in direct contact with γ—termed the DELSEED loop—is thought to play a critical role in torque transmission. We substituted all the DELSEED loop residues with alanine to diminish specific DELSEED loop-γ interactions and with glycine to disrupt the loop structure. All the mutants rotated unidirectionally with kinetic parameters comparable to those of the wild-type F_1, suggesting that the specific interactions between DELSEED loop and γ is not involved in cooperative interplays between the catalytic β-subunits. Glycine substitution mutants generated half the torque of the wild-type F_1, whereas the alanine mutant generated comparable torque. Fluctuation analyses of the glycine/alanine mutants revealed that the γ-subunit was less tightly held in the $\alpha_3\beta_3$-stator ring of the glycine mutant than in the wild-type F_1 and the alanine mutant. Molecular dynamics simulation showed that the DELSEED loop was disordered by the glycine substitution, whereas it formed an α-helix in the alanine mutant. Our results emphasize the importance of loop rigidity for efficient torque transmissions.

INTRODUCTION

ATP is the ubiquitous energy currency of a cell. A majority of ATP is produced by the oxidative phosphorylation process, wherein the terminal reaction, i.e., the ATP synthesis step, is catalyzed by the F_oF_1-ATP synthase (F_oF_1). As the term suggests, F_oF_1 is composed of two portions, F_o and F_1, both of which are rotary molecular motors (1–5). F_o is the membrane-integrated section of F_oF_1 and is driven by an electrochemical potential across the membrane (6). On the other hand, F_1-ATPase (F_1) is the water-soluble section, and its rotation is driven by ATP hydrolysis (7). The subunit composition of bacterial F_1 is $\alpha_3\beta_3\gamma\delta\varepsilon$, and the minimum functional unit acting as the ATP-driven motor is the $\alpha_3\beta_3\gamma$ subcomplex. The α- and β-subunits form a hexameric stator ring, wherein three α- and β-subunits are alternately arranged. The rotor shaft, γ, comprises a coiled-coil domain of antiparallel α-helices and a β-barrel domain. The coiled-coil domain is accommodated in the central cavity of the $\alpha_3\beta_3$-ring, whereas the β-barrel domain resides on the orifice of the $\alpha_3\beta_3$-ring. The catalytic reaction centers are located at each α–β interface and primarily on the β-subunits.

The three β-subunits undergo ATP hydrolysis in a highly cooperative manner to drive the unidirectional rotation of the γ-subunit in the counterclockwise direction when viewed from the F_o side (Fig. 1, *B*, *top*). The elementary step size of the rotation is 120° step, each of which is coupled with a single turnover of ATP hydrolysis. The 120° step can be further resolved into 80° and 40° substeps (8). In the crystal structure of the bovine heart mitochondrial F_1-ATPase (MF_1), the three β-subunits show distinctive differences in their bound ligands and conformations (9). In particular, one β-subunit (β_{TP}) binds to an ATP analog AMPPNP, another subunit (β_{DP}) binds to ADP, and the third subunit (β_{empty}) has no bound ligand.

Although the conformations of β_{TP} and β_{DP} are very similar, β_{empty} has a different conformation. β_{TP} and β_{DP} rotate the C-terminal domain inward, which pushes γ and closes the cleft of the catalytic site to enwrap the bound nucleotide. On the other hand, β_{empty} exhibits an open conformation that rotates the C-terminal domain outwards from γ. Thus, the three β-γ interactions are remarkably different in the manner in which they contact the C-terminal domain of β. The rotating motion of this domain upon the binding and release of the nucleotide was experimentally observed using NMR (10) and single-molecule imaging of the F_1 molecule during catalysis (11). It should be noted that the other major β-γ contact interface is located at the bottom of the $\alpha_3\beta_3$ cavity, and there are no distinctive conformational differences among the β-subunits. Instead, the bottom contact offers a smooth hydrophobic interface that is believed to act as the rotor holder.

The role of the β-γ contact at the C-terminal domain of β has been one of the points of focus for understanding the structural basis of the torque transmission mechanism. Fig. 1 shows this β-γ contact region; here, β has a short helical loop whose N- and C-terminal ends are connected by a long α-helix via a kink. This loop (residue number: 386–394 in Fig. 1 *A*) has a well-conserved amino-acid sequence of DELSEED, with a pronounced cluster of negatively charged residues (Fig. 1 *B*). In F_1 of the thermophilic

Submitted March 13, 2012, and accepted for publication June 25, 2012.

*Correspondence: hnoji@appchem.t.u-tokyo.ac.jp

Editor: Robert Nakamoto.

0006-3495/12/09/0970/9 $2.00

http://dx.doi.org/10.1016/j.bpj.2012.06.054

A

NAME	SEQUENCE
Wild -type	^{372}QTLQRYKELQDIIAILGMDELSD EDKLVVHRARR^{405}
Gly^{loop}	^{372}QTLQRYKELQDIIA^{386}GGGGGGGGG^{394}EDKLVVHRARR^{405}
Gly^{loop+5}	^{372}QTLQRYKELQDI^{384}GGGGGGGGGGGGGG^{397}LVVHRARR^{405}
Gly$^{loop+13}$	^{372}QTLQRYKE^{380}GGGGGGGGGGGGGGGGGGGGG^{401}RARR^{405}
Ala^{loop}	^{372}QTLQRYKELQDIIA^{386}AAAAAAAAA^{394}EDKLVVHRARR^{405}

B

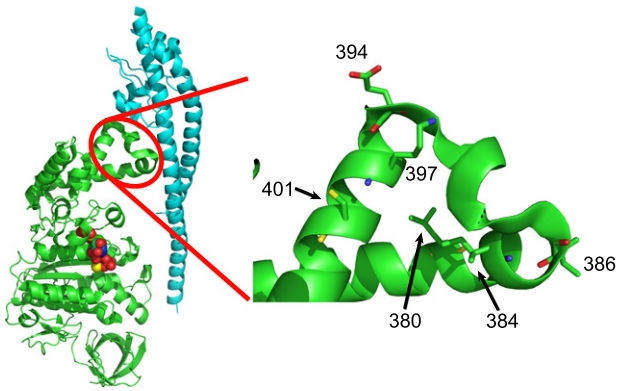

FIGURE 1 Sequence and structure of DELSEED loop. (*A*) Amino-acid sequences of the DELSEED loop and the mutants prepared in this study. Residues are numbered according to the TF_1 sequence. Residues Ile^{386} to Asp^{394} are defined as the DELSEED loop. (*B*) Crystal structure of the β-subunit (*green*) in its AMPPNP-bound form, i.e., β_{TP} form, and the γ-subunit (*cyan*) (PDB:2JDI). The positions of the both ends of glycine or alanine substitutions are shown (*sticks*) in the magnified images.

Bacillus PS3 (TF_1) used in this study, the corresponding sequence is DELSDED. For the sake of simplicity, hereafter, we refer to this loop as the DELSEED loop. In the crystal structure, the DELSEED loop is in contact with the positively charged amino-acid residues of γ that surround the γ-axis; these positively charged residues are termed the "ionic track" (12).

Therefore, the ionic track is assumed to play a role in guiding the DELSEED loop via electrostatic interactions. Molecular-dynamics (MD) studies have suggested that the interaction between the DELSEED loop and γ is important for torque transmission (13,14). The important role played by the DELSEED loop-γ contact in torque transmission was suggested by investigations on F_1 with truncated γ (15,16). In these investigations, large sections of the γ-axle were genetically removed, leaving behind only the interactions between the DELSEED loop and γ (15). The mutant F_1 still continued to exhibit unidirectional rotation despite the halving of the generated torque. In a subsequent work, the long C-terminal α-helix of the γ-subunit was completely removed, leaving behind the short N-terminal α-helix anchored in the $\alpha_3\beta_3$ cavity (16). However, the rotary properties of this mutant F_1 were not improved, suggesting that the N-terminal helix does not have a positive effect on the torque transmission. From these results, it has been proposed that the torque is principally transmitted via the DELSEED loop-γ contact.

Several mutagenesis studies have been carried out to investigate the role of the individual residues present in the DELSEED sequence in energy coupling and the rate-limiting step of the catalysis (17–20). A comprehensive mutagenesis study on the DELSEED residues was conducted by Hara et al. (20); they substituted all the negatively charged residues in the DELSEED sequence with alanine and studied the resultant AALSAAA mutant using a single-molecule rotation assay. Surprisingly, the mutant F_1 showed normal rotation behaviors, generating a rotary torque comparable to that of wild-type F_1. Therefore, the specific electrostatic interactions between the DELSEED sequence and the positively charged residues on γ are not necessary for the torque transmission. Subsequently, the negatively charged residues of the DELSEED sequence have been shown to be important for the interaction with the ε-subunit (21).

The DELSEED sequence itself occupies only the posterior half of the DELSEED loop (Fig. 1 *B*), and the role of the upstream sequence that has more direct contacts with γ in the torque transmission still needs to be clarified. Weber's group investigated the role of the DELSEED loop in a comprehensive manner. They generated a series of deletion mutants in which 3–7 consecutive residues of the DELSEED loop were removed (22). In some mutants, the catalytic activities were retained; however, the ratio of the ATP synthesis activity to the ATP hydrolysis activity decreased. This result suggests that an impaired coupling occurred between the proton translocation and the ATP hydrolysis/synthesis.

In a more recent study, they also showed that the deletion of three residues from the DELSEED loop and two turns of the N-terminal helix connected to the loop caused the ATP hydrolysis activity to uncouple from the proton translocation, as well as decreased the ATP synthesis activity. This observation suggests that there exists a critical length between β and γ that is required for the coupling of catalysis and rotation (23). The latest study on the DELSEED loop showed that the above truncation mutants decrease the torque, suggesting a role as the push-rod of the α-helix connected to the N-terminal end of the DELSEED loop (24). However, the specific interaction points of the DELSEED loop and γ were not completely eliminated in the case of individual mutants. The synergetic effects of the DELSEED residues on the torque transmission still remain unclear. Furthermore, the conformational and physical features that are required for efficient torque transmission remain elusive.

In this study, we attempted to elucidate the role of the DELSEED loop in torque transmission. We disrupted all the specific interactions of the DELSEED loop with the γ-subunit by substituting all nine loop-constituting residues

with alanine. Furthermore, to investigate the physical properties required for efficient torque transmission, we substituted all the DELSEED residues with glycine to disorder the helical structure of the DELSEED loop. One and two turns of the α-helices connected at the N- and C-terminal ends of the DELSEED loop were also substituted with glycine residues to further reduce the rigidity of the DELSEED loop. The rotations of the mutants were analyzed using a single-molecule rotation assay to determine the impact of the mutation on the torque transmission. Here, we discuss the obtained rotational properties based on the MD simulation data for the F_1 mutant.

MATERIALS AND METHODS

Preparation of F_1-ATPase

Four F_1-ATPase mutants from thermophilic *Bacillus* PS3 were prepared (Fig. 1). The subcomplex with the smallest number of mutations for which the rotation assay could be conducted—α(His_6 at N-terminus/C193S)$_3\beta$(His_{10} at N-terminus)$_3\gamma$(S108C/I211C)—was used as the wild-type F_1. It should be noted that these mutations do not affect the kinetic properties of F_1 (8). The mutants in which all the DELSEED loop residues were substituted with glycine (Gly^{loop}) or alanine (Ala^{loop}) were generated by PCR-based mutagenesis. The primers used for the mutagenesis are shown in the Supporting Material. We also replaced one and two turns in the α-helices that were connected at the N- and C-terminal ends of the DELSEED loop with glycine to produce Gly^{loop+5} and $Gly^{loop+13}$ mutants, respectively. For these mutants, a chemically synthesized oligonucleotide (GenScript, Piscataway, NJ) was inserted into the wild-type plasmid at the *Xho*I -*Pma*CI site. For all the mutants, sequences were designed on the basis of the codon usages for glycine and alanine in the *Escherichia coli* K12 strain. All the mutant preparations were confirmed by DNA sequencing.

Protein purification

Mutant and wild-type F_1 were expressed in *E. coli* JM103Δ*unc*. Cells were cultured in Terrific Broth medium at 37°C for at least 16 h and then harvested. F_1 was purified and biotinylated as described previously (8,25–27), with some minor modifications (the procedure is described in detail in the Supporting Material). During the entire purification process, the samples were treated at room temperature. The nucleotide-depletion procedure with ion-exchange chromatography was omitted. The purified F_1 was stored at room temperature.

Measurement of ATPase activity

The ATPase activity was measured at 25°C using the following ATP regenerating system: 2.5 mM phosphoenolpyruvate, 200 μg/mL pyruvate kinase, 50 μg/mL lactate dehydrogenase, 0.2 mM NADH, and the indicated ATP concentration in the ATPase assay buffer (20 mM 3-[*n*-morpholino] propanesulfonic acid-KOH (MOPS-KOH, pH 7.0), 50 mM KCl, and 5 mM $MgCl_2$) (28,29). The absorption at 340 nm was monitored by using a UV-visible spectrophotometer (VP-550; JASCO, Tokyo, Japan). The reaction was initiated by adding 6 μL of 1 μM F_1 (the final concentration of F_1 was 5 nM). Because none of the potentially bound nucleotides were depleted from the mutant F_1 values, lauryldodecylamine oxide (LDAO, catalogue No. 40236; Fluka Chemical, Milwaukee, WI) was added to the final concentration of 0.3% to monitor the fully activated F_1 activity. The ATPase activity of F_1 was determined from the slope of the absorption time course between 450 s and 550 s.

Rotation assay

A flow chamber for the rotation assay (<10 μL) was prepared as reported previously (7). Purified F_1 (100 pM–10 nM) was immobilized onto the Ni-NTA-modified glass surface via polyhistidine-tags (His-tags). The rotation assay for the Michaelis-Menten analysis was performed using a 60-nm gold colloid (30) as a nonfrictional rotation marker. After attaching the rotation marker, rotations were observed using a total internal reflection dark-field microscopy system (30) and recorded at 3000–18,000 frames/second (fps) using a high speed camera (FASTCAM-1024PCI; Photron, Tokyo, Japan). For the torque measurement, a streptavidin-coated magnetic bead (<0.3 μm) that was prepared from a commercially available magnetic bead (No. 30152105011150, <0.76 μm; Thermo Scientific, Barrington, IL) was used as a high-friction probe. Images were recorded at 1000 fps. The ATP (or ATPγS) concentration was adjusted by adding the rotation assay buffer (20 mM MOPS-KOH (pH 7.0), 50 mM KCl, and 5 mM $MgCl_2$ (when ATP was used, 1 mM phosphoenolpyruvate and 0.1 mg/mL pyruvate kinase were also added)). The rotation assay was performed at 25°C ± 1°C. The recorded images were analyzed using customized programs provided by R. Watanabe and K. Adachi.

Torque measurements

The torque (N) was determined from the rotation trajectories of the magnetic beads on the basis of the fluctuation theorem (31). It was calculated as $N = (k_BT/\Delta\theta)\bullet\ln[P(\Delta\theta)/P(-\Delta\theta)]$, where k_BT denotes the thermal energy and $P(\Delta\theta)$ denotes the probability density of the distance traveled within a given time. More than 100 steps per molecule were collected to increase the torque estimation accuracy.

MD simulations

MD simulations for the wild-type F_1 and the $Gly^{loop+13}$ and Ala^{loop} mutants were performed as described previously in Ito and Ikeguchi (32). For the initial structure for the simulations, we used a crystal structure at the catalytic dwell (PDB:2JDI) (33). Further, the AMP-PNP molecules in the β_{DP} and β_{TP} subunits of the original crystal structure were replaced with ATP. The structures were solvated in a box of water and neutralized with ions (Na^+ and Cl^-). The ion concentration was set to ~150 mM. The number of atoms used for the simulations is described in detail in Table S1 in the Supporting Material. Before sampling the MD trajectory, the entire system was equilibrated (the details of this procedure are described in the Supporting Material). All the simulations were carried out with the MD program MARBLE (34) using CHARMM22/CMAP (35,36) for proteins and TIP3P (37) for water, as the force-field parameters. Electrostatic calculations were performed using the particle-mesh Ewald method under periodic boundary conditions (38). The Lennard-Jones potential was truncated at 10 Å. Sampling MD simulations were performed for 30 ns, and the last 15 ns of the 30-ns simulation were used for the analysis. For contact analysis, residue pairs that were maintained at interatomic (except for hydrogen) distances of <4.5 Å were defined as being in contact. Only those residue pairs that appeared in >50% of the snapshots in the MD trajectory were detected.

RESULTS AND DISCUSSION

Rotation under unloaded condition

All the residues constituting the DELSEED loop were substituted with glycine or alanine to produce Gly^{loop} or Ala^{loop} mutants, respectively (Fig. 1). In addition to the glycine substitution, 1–2 turns of the α-helices connected at the N- and C-terminal ends of the DELSEED loop were

also substituted with glycine to further reduce the rigidity of the DELSEED loop; these mutants were termed Gly^{loop+5} and $Gly^{loop+13}$, respectively. The amino-acid sequences of the mutants are listed in Fig. 1 *A*. The mutants were expressed in *E. coli* and purified in accordance with previous reports (8,25–27). Electrophoresis analyses of the mutants showed that a fraction of the mutants lost the γ-subunit (see Fig. S2 in the Supporting Material). The fraction of γ-less F_1 ($\alpha_3\beta_3$ subcomplex) increased with the *Gly* substitution, suggesting that the DELSEED loop is somewhat responsible for holding the γ-subunit in the $\alpha_3\beta_3$ ring. However, all the mutants underwent the rotation assays. To observe the rotations, a gold colloid with a diameter of 60 nm was attached to the γ-subunit as a nonfrictional probe, which allowed us to determine the kinetic parameters of the rotations unaffected by the hydrodynamic friction on the probe (30). Fig. 2 *A* shows the time course of the rotation with 1 mM ATP.

All the mutants exhibited unidirectional rotations with continuous revolutions (usually over 20 revolutions), although the continuous rotation was interrupted with distinct pauses, as discussed below. These results imply that the fundamental competency of the rotary catalysis was retained in these mutant F_1, despite the large and extensive disruptions of the specific β-γ interactions. However, several characteristic behaviors were also observed. The rotational velocity of the $Gly^{loop+13}$ was evidently lower than that of the other mutants. All the mutants paused more frequently than the wild-type F_1, as shown in Fig. 2 *A*. These pauses may have occurred when the mutants were in the ADP-Mg inhibited form, because the angles of the pauses correspond to the catalytic angle (see Fig. S1) at which the ADP-inhibited F_1 pauses (39). It is interesting to note that $Gly^{loop+13}$ showed 120° back-steps more frequently than the wild-type F_1 and other mutants (see Fig. S3 *B*, *blue squares*). The probability of the occurrence of a back-step was ~0.5% for the wild-type F_1 and the other three mutants, whereas for $Gly^{loop+13}$, the back-step occurrence was up to 6%. Because the probability of the back-step varied significantly depending on the individual molecules, a precise analysis could not be achieved.

Michaelis-Menten kinetics

The rotations of all the mutants and the wild-type F_1 were observed at several ATP concentrations (Fig. 2 *B*, *solid circles*). The rotational velocity was determined from >30 successive revolutions. The back-steps were omitted from the analysis. The maximum velocities V_{max} and the Michaelis-Menten constants K_m (Fig. 2 *B*, *solid lines*) are summarized in Table 1. Both the kinetic parameters were comparable to those of the wild-type F_1. The apparent rate constants for the ATP binding of the mutants, i.e., $3V_{max}/K_m$, were comparable to that of the wild-type F_1. Thus, there

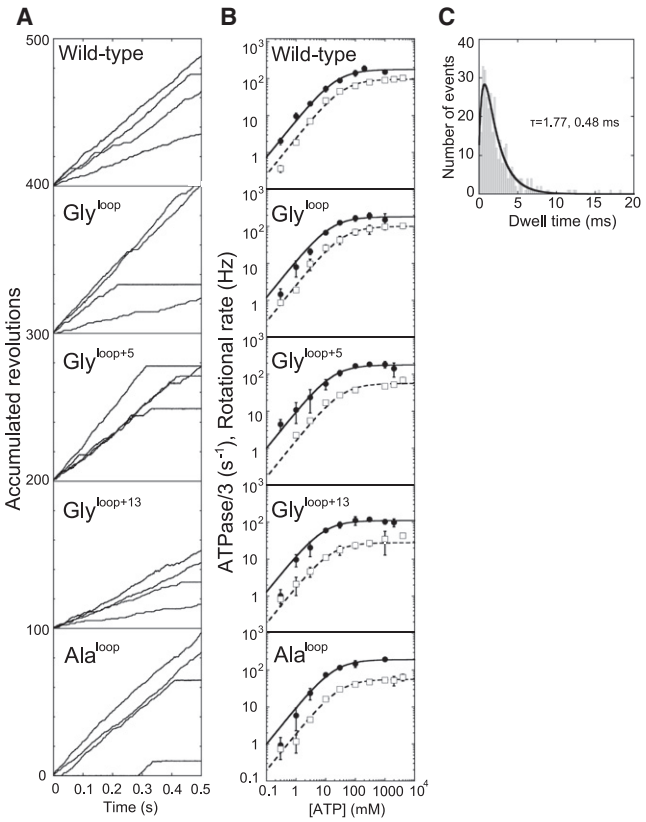

FIGURE 2 Time course of rotation and kinetic analyses of Ala and Gly mutants. (*A*) Time courses of rotation at 1 mM ATP. The probe used for the rotation was a 60-nm gold colloidal bead. The rotational velocity was determined from 30 continuous revolutions. (*B*) Rotational velocity and [ATP]. The average rotational rates and the estimated rotational rate from the ATPase activity (1/3 ATPase) are shown (*solid circles* and *open squares*, respectively). (*Error bars*) Standard deviations from at least four different molecules (*rotation assay*) or three independent measurements (*ATPase activity measurement*). (*Data points*) Fits using the Michaelis-Menten equation, $V = V_{max} \times [ATP]/(K_m + [ATP])$. The values of V_{max}, K_m, and the calculated k_{on}^{ATP} are summarized in Table 1. (*C*) (*Histogram*) Catalytic dwell of the $Gly^{loop+13}$ mutant at 1 mM ATP probed by a 60-nm gold colloid (2 molecules, 339 events). The histogram was fitted using the consecutive reaction model of two reactions. The time constants were determined to be 1.77 and 0.48 ms.

were no essential differences in the Michaelis-Menten kinetics between the mutants and the wild-type F_1.

The V_{max} of $Gly^{loop+13}$ was 40% lower than that of the wild-type F_1. The apparent k_{on}^{ATP} of $Gly^{loop+13}$ was also essentially the same as that of the wild-type F_1, because $Gly^{loop+13}$ had a correspondingly lower K_m than the other mutants. The time taken by $Gly^{loop+13}$ for the catalytic dwell comprising the hydrolysis-waiting time and the waiting time of P_i release was investigated. The catalytic dwell of the $Gly^{loop+13}$ mutant showed a distribution with a peak close to the first bin, as in the case of the distribution of the dwell time of the wild-type F_1 (8). The dwell-time distribution was well fitted with a consecutive reaction model that determined the time constants of the two reactions to be 0.5 ms and 1.8 ms (Fig. 2 *C*). These time constants were

TABLE 1 Kinetic parameters of Ala or Gly substitution mutants

Name	V_{max} (Hz) (V_{max}/3 (s^{-1}))	K_m^{ATP} (μM)	k_{on}^{ATP} (10^7 M^{-1} s^{-1})
Wild-type	180 ± 10	24 ± 7	2.2
	(97 ± 3)	(39 ± 6)	(0.25)
Gly^{loop}	180 ± 10	15 ± 4	3.7
	(100 ± 2)	(38 ± 4)	(0.27)
Gly^{loop+5}	180 ± 10	18 ± 5	3.0
	(50 ± 2)	(24 ± 3)	(0.21)
$Gly^{loop+13}$	110 ± 10	8.5 ± 2	3.9
	(28 ± 4)	(15 ± 5)	(0.19)
Ala^{loop}	190 ± 7	19 ± 2	3.0
	(56 ± 2)	(29 ± 6)	(0.19)

Kinetic parameters of the wild-type F_1 and all the mutants determined from the curve fitting of the data points in Fig. 2, *B* with Michaelis-Menten kinetics (*solid lines*) are summarized. The values determined from bulk measurements (Fig. 2, *B*, *dashed line*) are shown in parentheses. ATPase/3 (s^{-1}) represents the estimated rotational rate, assuming a coupling ratio of three ATPs per turn.

slightly higher than those of the catalytic dwell time of the wild-type F_1 (0.1–0.3 ms and 1.3 ms, respectively) (8,30,40,41). The total catalytic dwell of $Gly^{loop+13}$ was 2.3 ms, which was 1.4 times longer than the catalytic dwell of wild-type F_1. To summarize the above results, the rotational properties of the wild-type F_1 and all the mutants were essentially the same.

The ATP hydrolysis activity in the bulk solution was also measured for comparison. As mentioned above, the electrophoresis analysis suggests the mutants were less stable than the wild-type (see Fig. S2). Therefore, to avoid any further possible dissociation of the γ-subunit during the purification procedures, bound nucleotide depletion, which is required to measure the initial ATPase activity, was omitted from the purification procedure. Instead, the genuine activity was estimated from the steady-state ATPase activity in the presence of LDAO that is known to rescue F_1 from the ADP-inhibited form and activate the steady-state ATPase activity (42). Therefore, the ATPase assay in the presence of LDAO provides an ATPase rate close to the expected value from the rotation velocity; the one-third of the ATPase rate (ATPase/3) is expected to be equal to the rotation rate based on the coupling ratio of three ATPs per turn (27). All the mutants showed active ATPase activity (Fig. 2 *B*, *open squares*).

The Michaelis-Menten kinetic parameters for ATPase are summarized in Table 1 (shown in parentheses). The ATPase/3 rate of the wild-type F_1 was lower than the rotation rates as reported in our previous work (8). The apparent discrepancy was attributed to the fraction of inactive molecules unavoidably contaminating the sample. The mutants exhibited a larger deviation from the rotation rate than the wild-type. This large deviation seemingly suggests the mutants can make two or more steps of 120° rotation upon a single turnover of ATP hydrolysis. However, it is not possible, considering the pseudo-threefold symmetrical structure of F_1. The most feasible explanation is that the coexisting $\alpha_3\beta_3$ subcomplex of which ATPase rate is considerably slower than that of $\alpha_3\beta_3\gamma$ lowered the ensemble average of ATPase rate. In fact, the proportion of the $\alpha_3\beta_3\gamma$ complex to the total sample determined in the electrophoresis analyses showed a good correlation with the proportion of the ATPase/3 rate to the rotation rate (see Fig. S2 *C*). Based on these observations, we concluded that the coupling efficiency of the mutants was not different from that of the wild-type.

Measurement of torque

The torque of the mutants was measured to investigate the effects of mutations on the efficiency of the torque transmission. For this purpose, a magnetic bead with a diameter of ~300 nm was attached to F_1 as a frictional probe for the rotation of F_1. Under such load conditions, the angular velocity (ω) is determined by the hydrodynamic friction of the probe and the rotary torque generated by F_1: $\omega = N/\xi$, where N and ξ denote the torque and hydrodynamic frictional coefficient, respectively. However, because the size and shape of the magnetic beads were not uniform and the hydrodynamic frictional coefficient was not clear, we employed a recently developed method for torque measurement.

This method is based on the fluctuation theorem (31), which estimates the generated torque only from the rotation trajectory, without assuming the frictional coefficients of probes. The selection of rotating molecules that are unaffected by surface interactions is a prerequisite for precise torque determination. Because our early works (43), our principal criterion for this selection has been the threefold symmetry in the rotation trajectory. We observe the rotation under conditions where F_1 shows distinct pauses at three positions and then select rotating particles whose pause positions are 120° apart from the others. In this work, we added 1 mM of ATPγS to the solution, which retards the hydrolysis step and allows us to observe discrete 120° steps even under high-load and substrate-saturating conditions (44).

We then selected rotating molecules for analysis by following the above-mentioned criterion. The traces of the individual forward 120° steps were extracted from the time course of the rotation trajectory for the fluctuation theorem (31). Then, the ratio of the forward and backward movement probabilities, $[P(\Delta\theta)/P(-\Delta\theta)]$, over a certain time period within the 120° steps was calculated (see Fig. S3 *A*, *red squares*). The probability ratio was then plotted against $\Delta\theta$, and the torque was determined from the slope (Fig. 3). The torque of the wild-type F_1 driven by ATPγS was 32.6–43.2 pN·nm (torque in the 95% confidence interval), which was essentially the same as the torque of the ATP-driven rotation, i.e., 30.8–44.4 pN·nm. The torques of the mutants driven by ATPγS are summarized in Table 2. The Ala^{loop}-generated

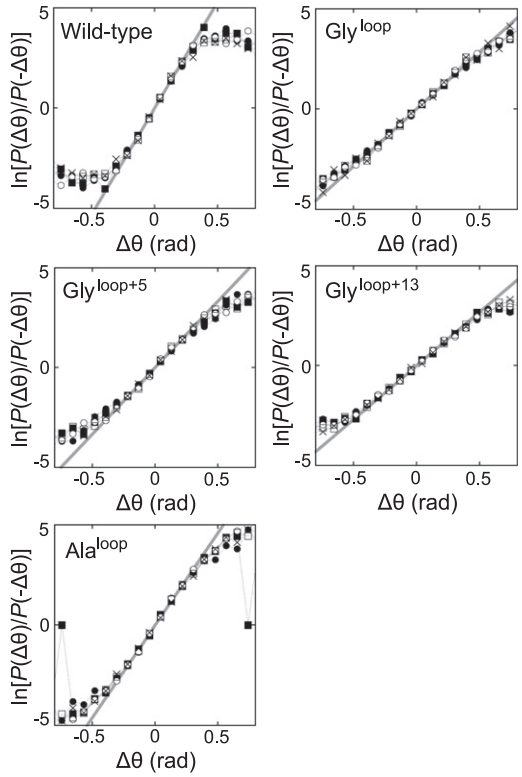

FIGURE 3 Torque determination of Ala and Gly mutants. The fluctuation theorem was employed for the measurement. The $\ln[P(\Delta\theta)/P(-\Delta\theta)]$ value is plotted against $\Delta\theta$ for $\Delta t = 3$ ms (*solid circles*), 4 ms (*solid squares*), 5 ms (*open circles*), 6 ms (*open squares*), and 7 ms (*cross*). The slope of this plot represents the torque/k_BT generated by F_1. The average torque was determined from a linear approximation of all the data points (*shaded line*) using a fitting width of ± 0.22 (rad). The results are summarized in Table 2.

torque of 32.9–41.0 pN·nm is comparable to that of the wild-type F_1; this suggests that the specific interactions of this region are dispensable for the torque transmission of the DELSEED loop.

On the other hand, the glycine-substituted mutants decreased the torque to ~60% of that of the wild-type F_1,

TABLE 2 Stepping torque

Name	Torque (pN nm)
Wild-type	32.6–43.2 (100%)
Gly^{loop}	21.7–27.3 (63%)
Gly^{loop+5}	22.1–30.9 (71%)
$Gly^{loop+13}$	20.9–27.9 (63%)
Ala^{loop}	32.9–41.0 (97%)

The 120° steps of each sample were observed under the condition of 1 mM ATPγS. The stepping torques were determined using the fluctuation theorem, where the Δt values were 5 ms. The torque of the 95% confidential interval was calculated from the mean value and variance. Over 1000 steps were collected in the case of the wild-type F_1 and the Gly^{loop} and Ala^{loop} mutants. The numbers of steps involved in Gly^{loop+5} and $Gly^{loop+13}$ were 580 and 440, respectively. The stepping-torque values were the data for 10 molecules in all the samples. The mean torque values in the parentheses were normalized using the value of the wild-type F_1 as the reference.

which suggests that the conformational rigidity of the DELSEED loop is important for the torque transmission. It is interesting to note that the kinetics of the ATPγS hydrolysis was also affected by the mutations. The time constant of the ATPγS hydrolysis for the mutants was 3–7 times greater than that for the wild-type F_1. The reason for this is unknown. The DELSEED loop might be involved in the conformational changes with the hydrolysis step.

Fluctuations in circumferential directions

In the glycine-substituted mutants, the glycine loop would be disordered, or at least, less ordered than in the wild-type F_1. A simple and feasible explanation for such a low torque of the glycine-substituted mutants is that the less-ordered loop is too soft to transfer the torque to γ from the nucleotide-binding domain of β. When the glycine-substituted DELSEED loop lost its rigidity, it no longer restricts the position of γ as much as the intact DELSEED loop, i.e., γ produces a larger fluctuation in a dwell state than in the wild-type F_1. To verify this, we measured the rotational stiffness of Ala^{loop} and $Gly^{loop+13}$ from the positional fluctuations of γ in a dwelling F_1. The stiffness of the wild-type F_1 was also measured under the same experimental conditions for the purpose of comparison. Rotation assays were carried out at 300 nM ATP using magnetic beads as rotation markers. The positional bead fluctuations during the ATP-waiting pauses were recorded at 1000 or 2000 fps.

It should be noted that a recording rate higher than 500 fps was fast enough to precisely measure the positional fluctuations of the magnetic beads attached to F_1 (45). The positional distributions in the circumferential direction were measured for eight molecules (*blue arrow* in Fig. 4 *A*). The standard deviation σ of the wild-type F_1 was 17°, which corresponds to a stiffness of 47 pN nm/radian. This value agrees well with the results of a previous experiment (45), thereby supporting the validity of the analysis. Ala^{loop} exhibited a very similar distribution ($\sigma = 19°$), whereas $Gly^{loop+13}$ showed a significantly wider distribution compared to that of the wild-type F_1 ($\sigma = 30°$) (Fig. 4 *B*). The stiffness was determined using the equipartition of the energy principle, $\frac{1}{2}\, k_BT = \frac{1}{2}\, k\sigma^2$, where κ represents the stiffness. The stiffness values of the wild-type F_1, Ala^{loop}, and $Gly^{loop+13}$ were 46.6, 41.6, and 14.8 pNnm/radian, respectively. The stiffness of $Gly^{loop+13}$ was obviously smaller, whereas Ala^{loop} did not show a significant difference from the wild-type F_1. Thus, the determined stiffness showed a good correlation with the torque. The stiffness determined from the rotary fluctuation was derived from two components—the rotary potential of the stator-embedded part of the γ-subunit and the stiffness of the external parts of the system, such as the protruding part of γ, His-tag, or streptavidin (45).

Because the external stiffness of $Gly^{loop+13}$ should be the same as that of the wild-type F_1, the smaller stiffness of

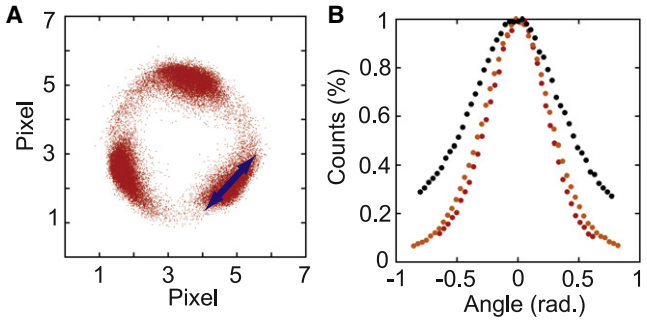

FIGURE 4 Fluctuation analysis of pausing mutant F_1. (*A*) Typical *x*-*y* trajectory of the rotation of wild-type F_1. The rotation was observed at 300 nM ATP. (*B*) Analysis of the fluctuations in circumferential directions. The probability distributions of the wild-type F_1 (*red*) and the $Gly^{loop+13}$ (*black*) and Ala^{loop} (*orange*) mutants are shown.

$Gly^{loop+13}$ indicated that its rotary potential was remarkably increased. This showed that the γ-subunit was not tightly held in the cavity of the $\alpha_3\beta_3$-stator ring of $Gly^{loop+13}$. This result is in good agreement with the contention that the glycine-substituted loop is considerably more flexible than the intact DELSEED loop.

MD simulation of $Gly^{loop+13}$ and Ala^{loop} mutants

To investigate the conformational state of the mutant DELSEED loops using another method, MD simulations were performed. These simulations were performed using all the atoms of the $\alpha_3\beta_3\gamma$ complex of MF_1 in the ground state (33) along with the surrounding water molecules and Mg^{2+}, as given in a previous work (32). The simulated structure reached equilibrium after ~15 ns, after which the root mean-square deviation from the initial structure did not show a distinct drift (data not shown). The data of the last 15 ns were then analyzed. Fig. 5 *A* shows the average conformational states of the β_{empty} forms of the wild-type F_1, Ala^{loop}, and $Gly^{loop+13}$ mutants in the last 15 ns of the simulation. The secondary structures of the β-subunits were determined using the define-secondary-structure-of-proteins (DSSP) analyses (46). As expected, the glycine loop did not have a stable α-helix structure (Fig. 5 *B*). On the contrary, it showed different conformations in the β_{TP}, β_{DP}, and β_{empty} forms (Fig. 5 *A* and see Fig. S4). Whereas, the glycine loop extended toward γ in β_{empty} (*back arrow* in Fig. 5 *A*), β_{DP} and β_{TP} showed a compact conformation of the glycine loop, in which the kink at the C-terminal end was obviously retracted (*arrows* shown in Fig. S4). These results suggest that the glycine loop was very flexible. The root mean-square fluctuation (RMSF) analysis also showed considerably high fluctuations at the glycine loop (Fig. 5 *D*), as compared with the alanine loop of Ala^{loop}.

In contrast to the glycine loop, Ala^{loop} maintained the α-helix structure, which was very similar to that of the wild-type F_1 (Fig. 5 *A* and see Fig. S4). This observation can be attributed to the relatively large side chain and the

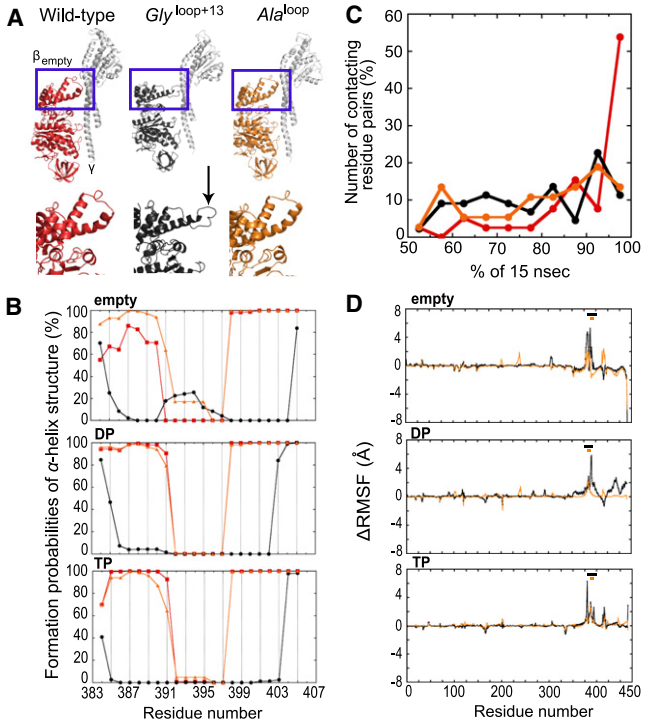

FIGURE 5 Molecular dynamics simulations of $Gly^{loop+13}$ and Ala^{loop}. (*A*) The average structures of β_{empty} during the last 15 ns of the simulations are shown (*ribbon representation*). The structures of β_{empty} in the wild-type F_1, $Gly^{loop+13}$, and Ala^{loop} are shown (*red*, *black*, and *orange*, respectively). The γ-subunit is also shown (*light gray*). (*Lower images*) Expanded views of the structures of the DELSEED loop regions (enclosed with *blue rectangles* in the *upper images*). (*B*) Results of DSSP analyses of β_{empty} (*empty*), β_{DP} (*DP*), and β_{TP} (*TP*). The probabilities of α-helix formation at individual residues of the DELSEED loop and adjacent regions in the wild-type F_1 (*red*), $Gly^{loop+13}$ (*black*), and Ala^{loop} (*orange*) are plotted. Residue numbers 384–405 in MF_1 correspond to 380–401 in TF_1. (*C*) (*Histograms*) Retention times of the specific contacts are shown. Bin-width is 5% of 15 ns (0.75 ns). The wild-type and $Gly^{loop+13}$ and Ala^{loop} mutants are represented (*red*, *black*, and *orange plots*, respectively). (*D*) ΔRMSF analysis of $Gly^{loop+13}$ (*black*) and Ala^{loop} (*orange*). The RMSF values of wild-type F_1 were subtracted from the RMSF values of $Gly^{loop+13}$ and Ala^{loop} to obtain the ΔRMSF values of β_{empty} (*empty*), β_{DP} (*DP*), and β_{TP} (*TP*). A positive ΔRMSF represents a larger fluctuation than that for the wild-type F_1, whereas negative values represent smaller fluctuations. (*Horizontal black* and *orange bars* in the figures represent the glycine- or alanine-substituted regions.)

low flexibility of the alanine residue. However, the specific interactions were not retained in $Gly^{loop+13}$ and Ala^{loop}. We measured the retention time of the specific contact between the residues of the DELSEED loop and γ (Fig. 5 *C*). Residue pairs with interatomic distances of <4.5 Å were defined as being in contact. When the residue pairs were in contact for >95% of the simulation time, the contact was defined as a stable contact. In the wild-type F_1, ~54% of the contacting pairs between the DELSEED loop and γ were stable. The remaining pairs were also in contact for >50% of the simulation time. On the other hand, only ~15% of the pairs were stably formed in $Gly^{loop+13}$ and Ala^{loop}. To estimate the nonspecific interactions, the total time of the interaction

with γ was also analyzed (see Fig. S5). Whereas the wild-type F_1 had a limited number of residues with stable interactions, which suggests a specific interaction, $Gly^{loop+13}$ had a larger number of interactions, particularly in the β_{empty} form. This finding indicates that the glycine/alanine loop interacts with the residues of the γ-subunit via many nonspecific interactions, and therefore can still transmit the torque to the γ-subunit.

CONCLUSION

The contact of the DELSEED loop with γ is responsible for torque transmission (15,16,47,48). In this study, we disrupted all the specific interactions between the DELSEED loop and γ by substituting the residues in the DELSEED loop with either glycine or alanine. All the mutant F_1 values still actively rotated unidirectionally. Although $Gly^{loop+13}$ had 120° back-steps, the probability of the forward step (94%) was considerably higher than that of the back-step (6%). Thus, the structural basis for the unidirectionality was essentially preserved in $Gly^{loop+13}$. Further, the Michaelis-Menten kinetic parameters (K_m and V_{max}) were not impaired by the alanine or glycine substitution at the DELSEED loop except for $Gly^{loop+13}$, which showed a slower V_{max}. These results suggest that the specific interaction between the DELSEED loop and γ do not play a critical role in the cooperative interplays among the three β-subunits or the kinetic power of F_1. In fact, using high-speed atomic force microscopy, we recently revealed that a β-subunit sequentially undergoes a conformational transition from an open to closed form in an isolated $\alpha_3\beta_3$ stator (49). This observation suggests that there is intrinsic cooperativity among the three β-subunits of a $\alpha_3\beta_3$ ring and that F_1 maintains normal cooperativity and catalytic power without any specific β-γ interactions.

This study also provided important insights into the torque transmission mechanism between the DELSEED loop of β and γ. Despite the extensive disruptions of the specific interactions at the contact between the DELSEED loop and γ, Ala^{loop} generated a torque comparable to that of the wild-type F_1. This result verified that the specific interactions are not required for the torque transmission between β and γ. On the other hand, all the glycine mutants had decreased torque. Both the experimental rotary fluctuation analysis and the MD simulation suggested that the glycine loop is significantly flexible. In this manner, our findings suggest that rigid body interaction is important for efficient torque transmission at the contact between the DELSEED loop and γ, as suggested by a theoretical work (50).

Usukura et al. (24) has reported interesting results: when the turns of the α-helix adjacent to the N-terminal end of the DELSEED loop were truncated, the mutant F_1s significantly decreased torque. From these results, they suggested that this α-helix acts as the push-rod of the β-subunit to induce the rotation of the γ -subunit. In this study, we substituted glycine for one and two turns of the α-helices connected to the N- and C-terminal ends of the DELSEED loop. However, this substitution did not cause an additional decrease in torque (compare the torques of Gly^{loop} and $Gly^{loop+13}$ in Table 2). This was probably because the glycine substitution did not induce significant shrinkage in the push-rod α-helix, as shown in our MD analysis (Fig. 5). When the role of the stiffness of the DELSEED loop and the length of the push-rod on the torque transmission are additive, a Gly^{loop} mutant with a shortened push-rod would show significantly low torque. In this manner, it would be revealed how a large torque could be extinguished using a mutagenic approach on the DELSEED loop, i.e., how a large torque is transmitted via the DELSEED loop. This awaits experimental verification.

SUPPORTING MATERIAL

Experimental Procedures section and Supporting Results, one table, five figures, and references (51,52) are available at http://www.biophysj.org/biophysj/supplemental/S0006-3495(12)00805-3.

We especially thank Dr. K. Hayashi for the useful discussions on torque measurements, as well as all the members of the laboratory of H.N. for their valuable discussions and advice. We thank Dr. P. Karagiannis for his proofreading of the manuscript.

We thank the Honjo International Scholarship Foundation and Global Centers of Excellence Program for young scientists for their financial support. This work was partially supported by Grants-in-Aid for Scientific Research from the Ministry of Education, Culture, Sports, Science and Technology, Japan (project 18074005) to H.N. as well as by a special education and research expenses grant to H.N. from the Ministry of Education, Culture, Sports, Science and Technology, Japan.

REFERENCES

1. Boyer, P. D. 1997. The ATP synthase—a splendid molecular machine. *Annu. Rev. Biochem.* 66:717–749.
2. Yoshida, M., E. Muneyuki, and T. Hisabori. 2001. ATP synthase—a marvelous rotary engine of the cell. *Nat. Rev. Mol. Cell Biol.* 2: 669–677.
3. Senior, A. E., S. Nadanaciva, and J. Weber. 2002. The molecular mechanism of ATP synthesis by F_1F_o-ATP synthase. *Biochim. Biophys. Acta.* 1553:188–211.
4. Nakamoto, R. K., J. A. Baylis Scanlon, and M. K. Al-Shawi. 2008. The rotary mechanism of the ATP synthase. *Arch. Biochem. Biophys.* 476:43–50.
5. Junge, W., H. Sielaff, and S. Engelbrecht. 2009. Torque generation and elastic power transmission in the rotary F_oF_1-ATPase. *Nature.* 459: 364–370.
6. Diez, M., B. Zimmermann, …, P. Gräber. 2004. Proton-powered subunit rotation in single membrane-bound F_oF_1-ATP synthase. *Nat. Struct. Mol. Biol.* 11:135–141.
7. Noji, H., R. Yasuda, …, K. Kinosita, Jr. 1997. Direct observation of the rotation of F_1-ATPase. *Nature.* 386:299–302.
8. Yasuda, R., H. Noji, …, H. Itoh. 2001. Resolution of distinct rotational substeps by submillisecond kinetic analysis of F_1-ATPase. *Nature.* 410:898–904.
9. Abrahams, J. P., A. G. Leslie, …, J. E. Walker. 1994. Structure at 2.8 Å resolution of F_1-ATPase from bovine heart mitochondria. *Nature.* 370:621–628.

10. Kobayashi, M., H. Akutsu, …, H. Yagi. 2010. Analysis of the open and closed conformations of the β-subunits in thermophilic F_1-ATPase by solution NMR. *J. Mol. Biol.* 398:189–199.

11. Masaike, T., F. Koyama-Horibe, …, T. Nishizaka. 2008. Cooperative three-step motions in catalytic subunits of F_1-ATPase correlate with 80° and 40° substep rotations. *Nat. Struct. Mol. Biol.* 15:1326–1333.

12. Ma, J., T. C. Flynn, …, M. Karplus. 2002. A dynamic analysis of the rotation mechanism for conformational change in F_1-ATPase. *Structure.* 10:921–931.

13. Pu, J., and M. Karplus. 2008. How subunit coupling produces the γ-subunit rotary motion in F_1-ATPase. *Proc. Natl. Acad. Sci. USA.* 105: 1192–1197.

14. Koga, N., and S. Takada. 2006. Folding-based molecular simulations reveal mechanisms of the rotary motor F_1-ATPase. *Proc. Natl. Acad. Sci. USA.* 103:5367–5372.

15. Furuike, S., M. D. Hossain, …, K. Kinosita, Jr. 2008. Axle-less F_1-ATPase rotates in the correct direction. *Science.* 319:955–958.

16. Mnatsakanyan, N., J. A. Hook, …, J. Weber. 2009. ATP synthase with its γ-subunit reduced to the N-terminal helix can still catalyze ATP synthesis. *J. Biol. Chem.* 284:26519–26525.

17. Lowry, D. S., and W. D. Frasch. 2005. Interactions between β-D372 and γ-subunit N-terminus residues γ-K9 and γ-S12 are important to catalytic activity catalyzed by *Escherichia coli* F_1F_0-ATP synthase. *Biochemistry.* 44:7275–7281.

18. Ketchum, C. J., M. K. Al-Shawi, and R. K. Nakamoto. 1998. Intergenic suppression of the γ-M23K uncoupling mutation in F_0F_1 ATP synthase by β-Glu-381 substitutions: the role of the β380DELSEED386 segment in energy coupling. *Biochem. J.* 330:707–712.

19. Scanlon, J. A., M. K. Al-Shawi, and R. K. Nakamoto. 2008. A rotor-stator cross-link in the F_1-ATPase blocks the rate-limiting step of rotational catalysis. *J. Biol. Chem.* 283:26228–26240.

20. Hara, K. Y., H. Noji, …, M. Yoshida. 2000. The role of the DELSEED motif of the β-subunit in rotation of F_1-ATPase. *J. Biol. Chem.* 275:14260–14263.

21. Hara, K. Y., Y. Kato-Yamada, …, M. Yoshida. 2001. The role of the βDELSEED motif of F_1-ATPase: propagation of the inhibitory effect of the ε-subunit. *J. Biol. Chem.* 276:23969–23973.

22. Mnatsakanyan, N., A. M. Krishnakumar, …, J. Weber. 2009. The role of the βDELSEED-loop of ATP synthase. *J. Biol. Chem.* 284:11336–11345.

23. Mnatsakanyan, N., S. K. Kemboi, …, J. Weber. 2011. The β-subunit loop that couples catalysis and rotation in ATP synthase has a critical length. *J. Biol. Chem.* 286:29788–29796.

24. Usukura, E., T. Suzuki, …, M. Yoshida. 2012. Torque generation and utilization in motor enzyme F_oF_1-ATP synthase: half-torque F_1 with short-sized pushrod helix and reduced ATP synthesis by half-torque F_oF_1. *J. Biol. Chem.* 287:1884–1891.

25. Adachi, K., H. Noji, and K. Kinosita, Jr. 2003. Single-molecule imaging of rotation of F_1-ATPase. *Meth. Enzymol.* 361:211–227.

26. Noji, H., D. Bald, …, K. Kinosita, Jr. 2001. Purine but not pyrimidine nucleotides support rotation of F_1-ATPase. *J. Biol. Chem.* 276:25480–25486.

27. Rondelez, Y., G. Tresset, …, H. Noji. 2005. Highly coupled ATP synthesis by F_1-ATPase single molecules. *Nature.* 433:773–777.

28. Adachi, K., R. Yasuda, …, K. Kinosita, Jr. 2000. Stepping rotation of F_1-ATPase visualized through angle-resolved single-fluorophore imaging. *Proc. Natl. Acad. Sci. USA.* 97:7243–7247.

29. Kato, Y., T. Sasayama, …, M. Yoshida. 1995. Analysis of time-dependent change of *Escherichia coli* F_1-ATPase activity and its relationship with apparent negative cooperativity. *Biochim. Biophys. Acta.* 1231: 275–281.

30. Ueno, H., S. Nishikawa, …, H. Noji. 2010. Simple dark-field microscopy with nanometer spatial precision and microsecond temporal resolution. *Biophys. J.* 98:2014–2023.

31. Hayashi, K., H. Ueno, …, H. Noji. 2010. Fluctuation theorem applied to F_1-ATPase. *Phys. Rev. Lett.* 104:218103.

32. Ito, Y., and M. Ikeguchi. 2010. Structural fluctuation and concerted motions in F_1-ATPase: a molecular dynamics study. *J. Comput. Chem.* 31:2175–2185.

33. Bowler, M. W., M. G. Montgomery, …, J. E. Walker. 2007. Ground state structure of F_1-ATPase from bovine heart mitochondria at 1.9 Å resolution. *J. Biol. Chem.* 282:14238–14242.

34. Ikeguchi, M. 2004. Partial rigid-body dynamics in NPT, NPAT and NPγT ensembles for proteins and membranes. *J. Comput. Chem.* 25:529–541.

35. MacKerell, Jr., A. D., M. Feig, and C. L. Brooks, 3rd. 2004. Extending the treatment of backbone energetics in protein force fields: limitations of gas-phase quantum mechanics in reproducing protein conformational distributions in molecular dynamics simulations. *J. Comput. Chem.* 25:1400–1415.

36. MacKerell, A. D., D. Bashford, …, M. Karplus. 1998. All-atom empirical potential for molecular modeling and dynamics studies of proteins. *J. Phys. Chem. B.* 102:3586–3616.

37. Jorgensen, W. L., J. Chandrasekhar, …, M. L. Klein. 1983. Comparison of simple potential functions for simulating liquid water. *J. Chem. Phys.* 79:926–935.

38. Essmann, U., L. Perera, …, L. G. Pedersen. 1995. A smooth particle mesh Ewald method. *J. Chem. Phys.* 103:8577–8593.

39. Hirono-Hara, Y., H. Noji, …, M. Yoshida. 2001. Pause and rotation of F_1-ATPase during catalysis. *Proc. Natl. Acad. Sci. USA.* 98:13649–13654.

40. Watanabe, R., R. Iino, and H. Noji. 2010. Phosphate release in F_1-ATPase catalytic cycle follows ADP release. *Nat. Chem. Biol.* 6: 814–820.

41. Adachi, K., K. Oiwa, …, K. Kinosita, Jr. 2007. Coupling of rotation and catalysis in F_1-ATPase revealed by single-molecule imaging and manipulation. *Cell.* 130:309–321.

42. Jault, J. M., T. Matsui, …, W. S. Allison. 1995. The $\alpha3\beta3\gamma$-complex of the F_1-ATPase from thermophilic *Bacillus* PS3 containing the α-D261N substitution fails to dissociate inhibitory MgADP from a catalytic site when ATP binds to noncatalytic sites. *Biochemistry.* 34:16412–16418.

43. Yasuda, R., H. Noji, …, M. Yoshida. 1998. F1-ATPase is a highly efficient molecular motor that rotates with discrete 120° steps. *Cell.* 93:1117–1124.

44. Shimabukuro, K., R. Yasuda, …, M. Yoshida. 2003. Catalysis and rotation of F_1 motor: cleavage of ATP at the catalytic site occurs in 1 ms before 40° substep rotation. *Proc. Natl. Acad. Sci. USA.* 100:14731–14736.

45. Okuno, D., R. Iino, and H. Noji. 2010. Stiffness of γ-subunit of F_1-ATPase. *Eur. Biophys. J.* 39:1589–1596.

46. Kabsch, W., and C. Sander. 1983. Dictionary of protein secondary structure: pattern recognition of hydrogen-bonded and geometrical features. *Biopolymers.* 22:2577–2637.

47. Hossain, M. D., S. Furuike, …, K. Kinosita, Jr. 2006. The rotor tip inside a bearing of a thermophilic F_1-ATPase is dispensable for torque generation. *Biophys. J.* 90:4195–4203.

48. Hossain, M. D., S. Furuike, …, K. Kinosita, Jr. 2008. Neither helix in the coiled coil region of the axle of F_1-ATPase plays a significant role in torque production. *Biophys. J.* 95:4837–4844.

49. Uchihashi, T., R. Iino, …, H. Noji. 2011. High-speed atomic force microscopy reveals rotary catalysis of rotorless F_1-ATPase. *Science.* 333:755–758.

50. Wang, H., and G. Oster. 1998. Energy transduction in the F_1 motor of ATP synthase. *Nature.* 396:279–282.

51. Sali, A., and T. L. Blundell. 1993. Comparative protein modeling by satisfaction of spatial restraints. *J. Mol. Biol.* 234:779–815.

52. DeLano, W. L. 2002. The PyMOL Molecular Graphics System. DeLano Scientific, San Carlos, CA 51.